heritage

MDPI

Article

Volcanic Pozzolan from the Phlegraean Fields in the Structural Mortars of the Roman Temple of Nora (Sardinia)

Simone Dilaria [1,2], Caterina Previato [1,*], Jacopo Bonetto [1,2], Michele Secco [1,2], Arturo Zara [1], Raffaella De Luca [3] and Domenico Miriello [3]

[1] Department of Cultural Heritage: Archaeology, History of Art, Cinema and Music (DBC), University of Padua, Piazza Capitaniato 7, 35139 Padua, Italy
[2] Inter-Departmental Research Centre for the Study of Cement Materials and Hydraulic Binders (CIRCe), University of Padova, Via Giovanni Gradenigo 6, 35131 Padua, Italy
[3] Department of Biology, Ecology and Earth Sciences (DiBEST), University of Calabria, Via P. Bucci, 87036 Arcavacata di Rende, Italy
* Correspondence: caterina.previato@unipd.it

Abstract: In this paper, we discuss the presence of volcanic pozzolans in the structural mortars of the Roman Temple of Nora in Sardinia (3rd c. AD), represented by pyroclastic rocks (pumices and tuffs) employed as coarse and fine aggregates. The provenance of these materials from the Phlegraean Fields was highlighted through a multi-analytical approach, involving Polarized Light Microscopy on thin sections (PLM), Scanning Electron Microscopy with Energy Dispersive Spectroscopy (SEM-EDS), Quantitative Phase Analysis by X-ray Powder Diffraction (QPA-XRPD), and X-ray Fluorescence (XRF) investigations. These volcanic pozzolans, outcropping in the Bay of Naples between Pozzuoli and the Vesuvius, are traditionally associated with the *pulvis puteolana*, the famous pozzolanic ash prescribed by Vitruvius and Pliny in order to confer strength and waterproofing capabilities to ancient concretes. This is the first evidence of the trade of this volcanic material from the Neapolitan area to Sardinia, starting at least by the Middle Imperial Age. The use of the *pulvis puteolana* in the Roman Temple of Nora seems primarily targeted to strengthen aboveground masonries, while waterproofing capabilities were not strictly pursued. This opens new questions about the construction reasons for which the demand and commercialization for this product was intended.

Keywords: volcanic pozzolan; *pulvis puteolana*; Phlegraean pumices and tuffs; X-ray fluorescence; discriminant analysis; Roman mortars and binder; provenance analysis; Nora; Sardinia

Citation: Dilaria, S.; Previato, C.; Bonetto, J.; Secco, M.; Zara, A.; De Luca, R.; Miriello. D. Volcanic Pozzolan from the Phlegraean Fields in the Structural Mortars of the Roman Temple of Nora (Sardinia). *Heritage* **2023**, *6*, 567–587. https://doi.org/10.3390/heritage6010030

Academic Editors: João Pedro Veiga

Received: 27 December 2022
Revised: 4 January 2023
Accepted: 6 January 2023
Published: 10 January 2023

Copyright: © 2023 by the authors. Licensee MDPI, Basel, Switzerland. This article is an open access article distributed under the terms and conditions of the Creative Commons Attribution (CC BY) license (https://creativecommons.org/licenses/by/4.0/).

1. Introduction

Ancient societies did not have the pyrotechnological awareness and the adequate technology for the production of Portland cement, since this requires fusion temperatures of about 1450 °C to sinter the materials into clinker. Nevertheless, Romans were able to produce highly cohesive mortar-based materials by mixing an "aerial" lime, obtained by the calcination of carbonate rocks in wood-fired limekilns at relatively low temperatures (~850 °C), with natural and artificial pozzolanic materials. Terracotta fragments and powders, organic ashes, and, especially, pyroclastic rocks were the most common pozzolanas used in antiquity [1].

All these materials are rich in reactive silica (SiO_2) and alumina (Al_2O_3), which, when blended in aqueous solution, can interact with calcium hydroxide (portlandite, $Ca(OH)_2$), inducing the dissolution of the silicate or aluminate phases to form a series of reaction products (calcium-silicate-hydrates C-S-H and calcium-aluminate-hydrates C-A-H) in a way that closely resembles the anthropogenic phases occurring in modern Portland

cement [2–4]. By chemically reacting with lime, pozzolanic materials can improve the mechanical and hydraulic properties of aerial lime-based mortars.

The most famous pozzolan of the Roman Age is the *pulvis puteolana*. As reported by Vitruvius (2.6.1 and 5.12.2), this was considered a "prodigious powder", outcropping in a broad region, ranging from Baia and Cuma to the Vesuvius and the Sorrentine Peninsula. The adjective "puteolana" was actually used for the very first time by Pliny (35.166), locating the provenance area of the material in the proximity of the ancient town of *Puteoli* (today, Pozzuoli, north of Naples). Geologically, *pulvis puteolana* is identified with the pyroclastic rocks outcropping around the Bay of Naples, from the Phlegraean Fields to Somma-Vesuvius [5].

According to the ancient treaties, this *pulvis* can provide excellent structural characteristics and waterproofing properties to ancient concretes, and it was recommended, in particular by Pliny, for the construction of *opus caementicium* maritime piers (Vitr. 2.6.1; Plin. 35.166). In fact, the presence of volcanic pozzolan from the Bay of Naples in the piers of some of the main harbors of the Roman Empire has been demonstrated by recent research [5–7].

However, Vitruvius (2.6.1) clearly indicated *pulvis puteolana* to be primarily employed in a broad range of buildings for masonry reinforcement (*non modo ceteris aedificiis praestat firmitates*), and only secondarily in maritime architecture (*sed etiam moles cum struuntur in mari, sub aqua solidescunt*) [8]. This interpretation of the ancient text has been little considered in the geoarchaeological literature so far [5,9–12].

The data presented in this paper report a case of utilization of the *pulvis puteolana* as intended in the first part of the aforementioned Vitruvian statement. In fact, in the Roman Temple of Nora (Southern Sardinia), dated to the Middle Imperial Age (3rd c. AD), we observed the presence of pumices and tuffs employed as pozzolanic aggregate in the structural mortars of the foundational and above-ground masonries.

The provenance of these materials from the Phlegraean Fields in the Bay of Naples was demonstrated through a multi-analytical approach, involving PLM, XRPD, and XRF investigations.

Therefore, the use of the *pulvis puteolana* in the Roman Temple of Nora seems primarily targeted to structural strengthening, while waterproofing was not intentionally pursued.

2. Context of Research and Sampling

2.1. The Roman Temple of Nora and Its Construction Techniques

Nora (Sardinia, Italy) is located on a large peninsula at the south-western edge of the Gulf of Cagliari (Figure 1a). The early Phoenician settlement dates back to the mid-8th c. BC [13] and it developed into an urban center during the Punic period (late 6th–5th c. BC) [14].

In 227 BC, Sardinia became a Roman province, and in the second half of the 1st c. BC, Nora acquired the *ius civium Romanorum* (Roman citizenship) as *municipium* [15], but the climax of its growth was reached in the 3rd c. AD, also thanks to the monumental refurbishment of the city during the Severan age [16].

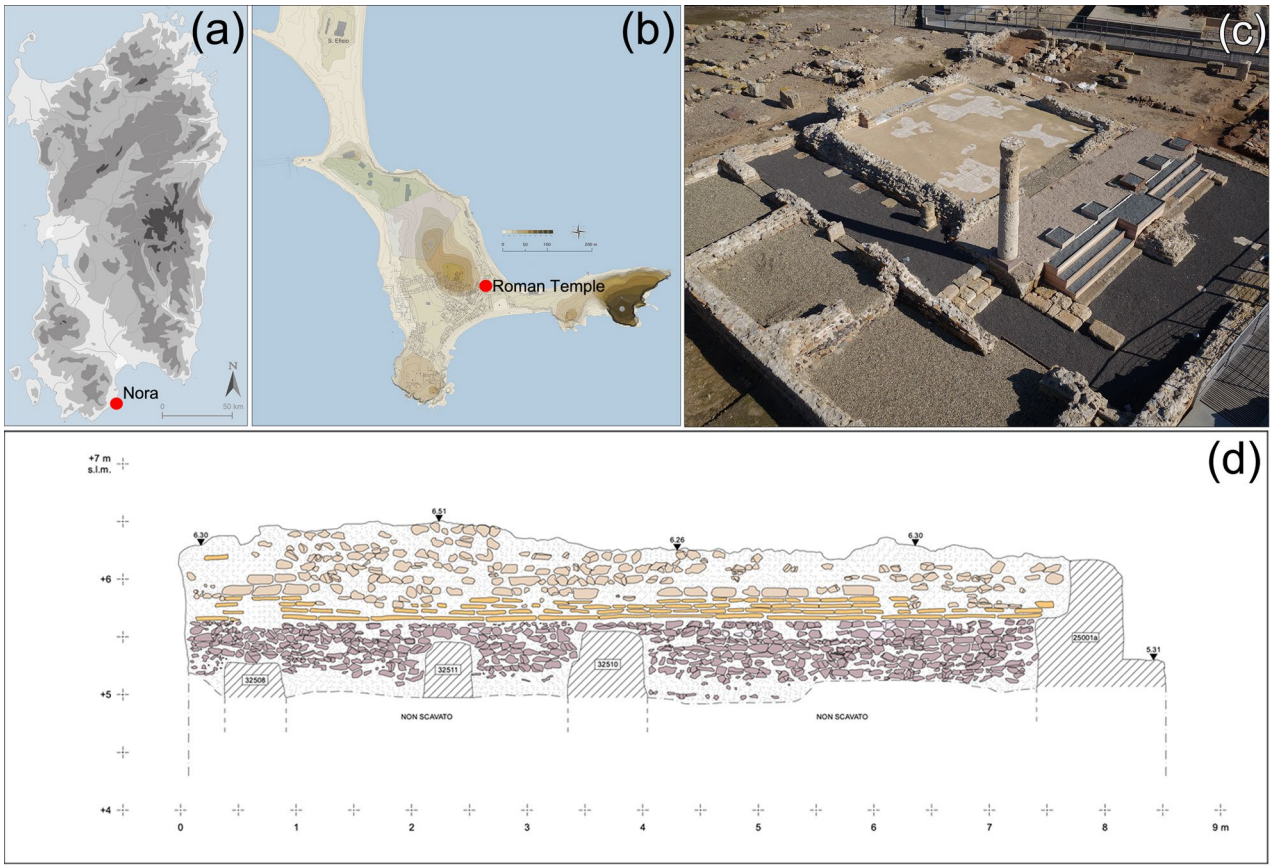

Figure 1. The Roman Temple of Nora: (**a**) Location of Nora in Sardinia; (**b**) position of the Roman Temple in Nora; (**c**) actual state of the Roman Temple after the restoration; (**d**) drawing of the facing of one of the walls of the *cella*, highlighting the different building materials used in foundations and masonry walls.

The Roman Temple of Nora, situated in the central part of the ancient city (Figure 1b), is a sacred building dating back to 225–250 AD and organized as a small sanctuary, probably dedicated to the Imperial cult [17,18]. The consecrated space was enclosed by a high wall with a monumental access, introduced to a courtyard where the *cella* with a hexastyle pronaos was placed; two doors in the back wall of the *cella* give access to a small rectangular room, the most sacred part of the sanctuary. West of the *cella* there were three small rooms, whose function is not clear, but they can be interpreted as ancillary spaces for the sanctuary activities (Figure 1c). The Roman Temple presents the typical construction techniques employed in the monumental buildings of Nora built between the late 2nd c. and the 3rd c. AD [19]. The foundations consist of irregular-shaped stones (mostly andesites/dacites) placed in rows and bounded with lime mortar; the raised masonry walls present a facing composed of courses of local calcarenite blocks alternated with bricks and a core made in *opus caementicium* (Figure 1d). The thickness of the *cella* masonries is 85–100 cm at the foundations, while it is around 60–80 cm in the walls. The walls of the western rooms have a lower thickness (foundations: 55–60 cm; above-ground portions: 45–55 cm).

2.2. The Sampling

Eight samples of mortars and nine samples of coarse volcanic rocks, visually recognized as incompatible with the local volcanic lithotypes, mainly constituted by compact andesite/dacite lavas, were collected for laboratory analysis from the masonries and foundations of the temple (Table 1, Figure 2a). Cross-sections of the coarse volcanic clasts allowed some fragments of tuffs (Figure 3a) and some vesicular and compact pumices (Figure 3b–f) to be distinguished. Specifically, all coarse porous volcanic rocks come from the

walls of the main *cella* of the temple (Figure 2b–e). Regarding the mortars, four samples were collected from the cores of the thick perimetral walls of the *cella*, where sub-centimetric volcanic clasts, resembling the aspect of the coarse ones, were macroscopically identified (Figure 2f). The remaining mortars were collected from different walls of the western rooms, where these volcanic aggregates were not macroscopically detected (Figure 2g).

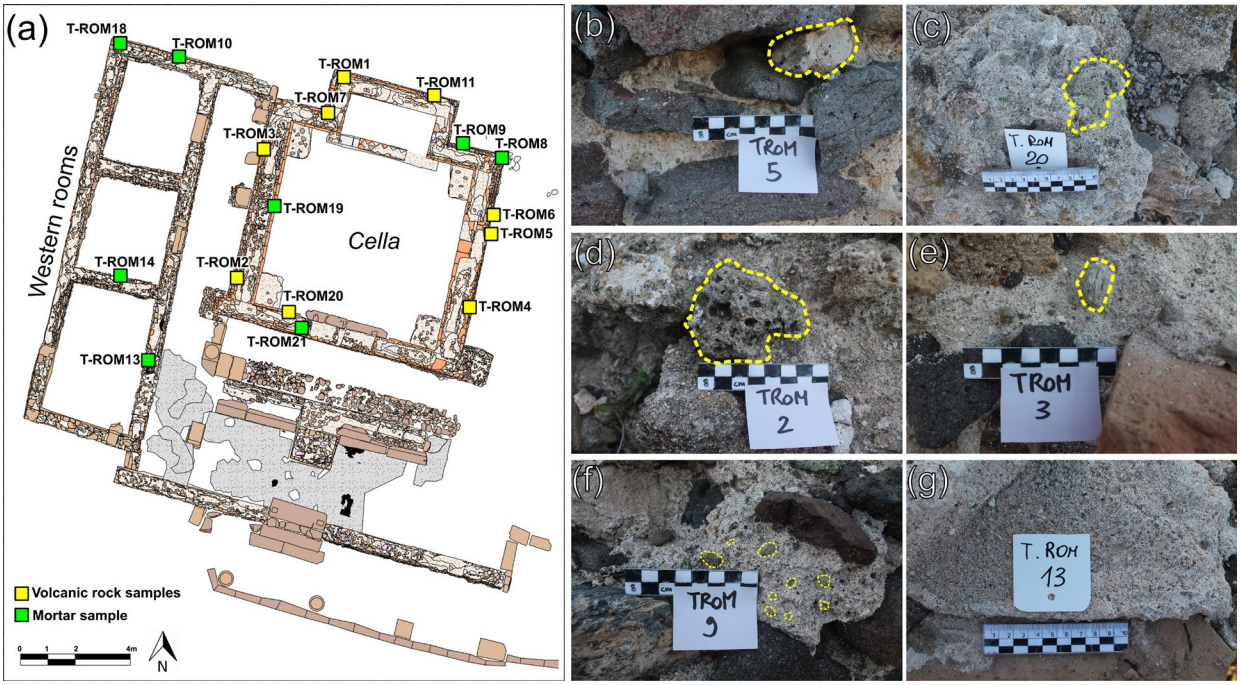

Figure 2. The sampling in the Roman Temple of Nora: (**a**) planimetric distribution of the analyzed samples of mortars and volcanic rocks; (**b**–**e**) coarse clasts of volcanic rocks, highlighted by dashed yellow line; (**f**,**g**) the sampling of the mortars from the *cella* and the western rooms.

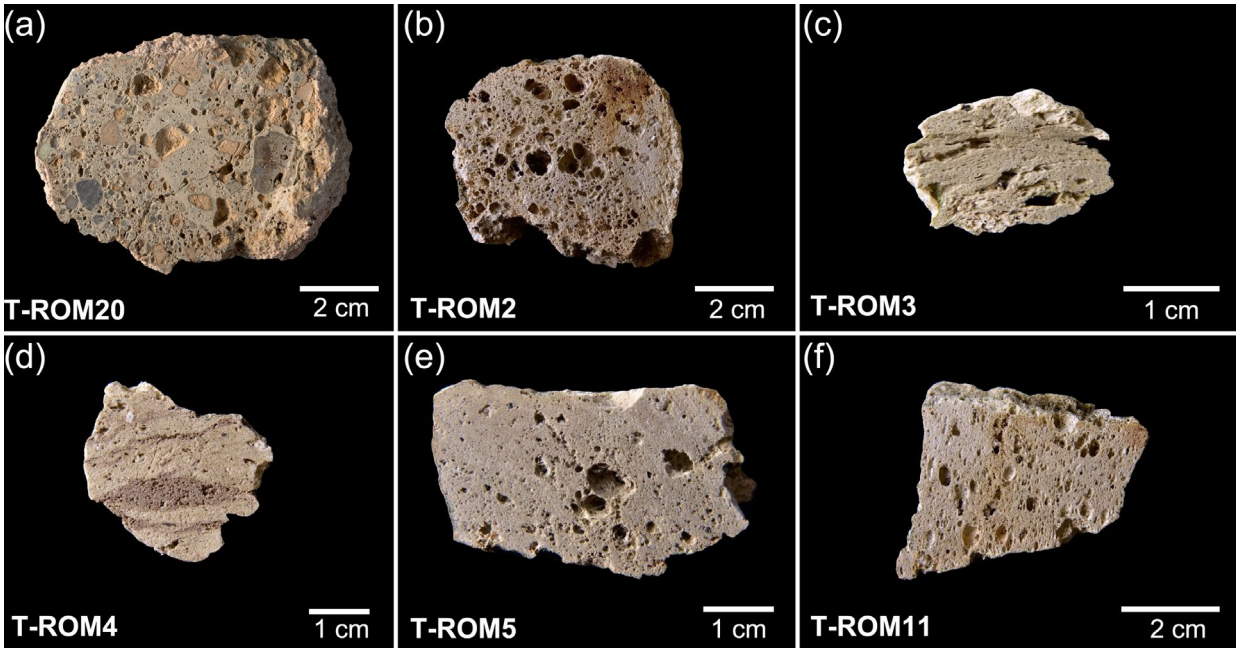

Figure 3. Coarse clasts of porous volcanic rocks after the petrographic cut: (**a**) tuff; (**b**–**f**) vesicular and compact pumices.

Table 1. List of the analyzed samples and positions.

Sample	Type	Position
T-ROM1	Tuff	Foundation of the *cella* (NW)
T-ROM2	Pumice	Outer wall of the *cella* (W)
T-ROM3	Pumice	Outer wall of the *cella* (W)
T-ROM4	Pumice	Foundation of the *cella* (E)
T-ROM5	Pumice	Foundation of the *cella* (E)
T-ROM6	Pumice	Foundation of the *cella* (E)
T-ROM7	Pumice	Outer wall of the *cella* (NW)
T-ROM8	Mortar	Outer wall of the *cella* (NE)
T-ROM9	Mortar	Outer wall of the *cella* (NE)
T-ROM10	Mortar	Outer wall of the western rooms (N)
T-ROM11	Pumice	Outer wall of the *cella* (N)
T-ROM13	Mortar	Outer wall of the western rooms (E)
T-ROM14	Mortar	Inner wall of the western rooms (E)
T-ROM18	Mortar	Outer wall of the western rooms (N)
T-ROM19	Mortar	Inner wall of the *cella* (W)
T-ROM20	Tuff	Inner wall of the *cella* (S)
T-ROM21	Mortar	Outer wall of the *cella* (S)

3. Analytical Techniques

3.1. PLM

All mortar samples were analyzed by Polarized Light Microscopy (PLM) in transmitted light (TL) on 30 μm thin sections under a Leica DM750 P operating with an integrated digital camera FLEXACAM C1 (Leica Microsystems, Heerbrugg, Switzerland). In order to describe the texture and petro-mineralogical characteristics of the mortars, the PLM analysis was carried out according to the analytical procedures described in the Standard UNI 11176:2006 "Cultural heritage—Petrographic description of a mortar". The quantification of the porosity rate and of the binder to aggregate proportions was evaluated for each sample through digital image analysis performed using Image-J software (v. 1.51j8) [20].

3.2. SEM-EDS

SEM-EDS analysis was performed on the 30 μm thin sections with a COXEM EM 30AX plus scanning electron microscope working with a Tungsten filament (W) ((Yuseong-gu, Daejeon, South Korea), equipped with SE and BSE detectors (Solid type 4 Channel) and an energy dispersive X-ray detector (EDX) EDAX Element-C2B (EDAX, Mahwah, USA). Before the analysis, thin sections were carbon coated. These analyses were carried out to (a) analyze the chemical composition of the binders; (b) determine the formation of hydraulic phases in the matrices, through the calculation of the cementation index (C.I.), according to [21,22]; (c) describe the extent of reaction processes of the volcanic pozzolans with the lime.

3.3. QPA-XRPD

QPA-XRPD analyses were performed on the coarse clasts of volcanic pozzolans. XRPD profiles were collected using a Bragg–Brentano θ-θ diffractometer (PANalytical X'Pert PRO, Cu Kα radiation, 40 kV and 40 mA) equipped with a real-time multiple strip (RTMS) detector (Malvern PANalytical, Malvern, UK). Data acquisition was performed by operating a continuous scan in the range 3–85 [◦2θ], with a virtual step scan of 0.02 [◦2θ]. Diffraction patterns were interpreted with X'Pert HighScore Plus 3.0 software by PANalytical (Malvern PANalytical, Malvern, UK), qualitatively reconstructing mineral profiles of the compounds by comparison with PDF databases from the International

Centre for Diffraction Data (ICDD). Then, quantitative phase analysis (QPA) was performed using the Rietveld method [23]. Refinements were carried out with TOPAS software (version 4.1) by Bruker AXS. The correct quantification of smectite clays observed in some samples was accomplished by adopting a BGMN-Profex software (J. Bergmann, Dresden, Germany) with dedicated fitting functions for Rietveld refinements of these phases [24]. The quantification of both crystalline and amorphous content was obtained through the addition of 20 wt% of zincite to the powders as an internal standard. The observed Bragg peaks in the powder patterns have been modelled through a pseudo-Voigt function, fitting the background with a 12 coefficients Chebyshev polynomial. For each mineral phase, lattice parameters, Lorentzian crystal sizes, and scale factors have been refined. Although samples were prepared with the backloading technique to minimize the preferred orientation of crystallites a priori, any residual preferred orientation effect was modelled during the refinement with the March Dollase algorithm [25]. The starting structural models for the refinements were taken from the International Crystal Structure Database (ICSD).

3.4. XRF

XRF analysis was adopted in order to characterize the chemical composition of major and trace elements of the sampled volcanic rocks. The analysis was performed with a WDS Panalytical Zetium sequential spectrometer (Malvern PANalytical, Malvern, UK), operating under vacuum conditions and equipped with a 2.4 kW Rh tube. Samples were calcined to determine their Loss On Ignition (L.O.I.) by placing them in a muffle furnace at 860 °C for about 20 min, and then at 980 °C for about 2 h. Samples for XRF analysis were then prepared in beads using lithium tetraborate (Li2B4O7) as a flux at a dilution of 1:10, and melting was carried out using a Claisse Eagon 2 bead mill (maximum temperature achieved of about 1150 °C) (Malvern PANalytical, Malvern, UK). The calculated major elements are Si, Ti, Al, Fe, Mn, Mg, Ca, Na, K, and P (expressed as a percentage of the relative oxide). The L.O.I. was calculated separately. The calculated trace elements (expressed in ppm) are Sc, V, Cr, Co, Ni, Cu, Zn, Ga, Rb, Sr, Y, Zr, Nb, Ba, La, Ce, Nd, Pb, Th, and U. Instrumental precision (defined by repeated analysis on the same sample) is within 0.6 % relative for major elements, and within 3.0% relative for trace elements. Detection limits for Al, Mg, and Na are within 0.01%, within 0.2% for Si, and within 0.005% for Ti, Fe, Mn, Ca, K, and P. Limits for trace elements are (in ppm): Sc = 3, V = 5, Cr = 6, Co = 3, Ni = 3, Cu = 3, Zn = 3, Ga = 3, Rb = 3, Sr = 3, Y = 3, Zr = 3, Nb = 3, Ba = 10, La = 10, Ce = 10, Nd = 10, Pb = 5, Th = 3, U = 3.

4. Results

4.1. Mortars Characterization

Two groups of mortars were defined after PLM analysis (Table 2).

Table 2. Petrographic and textural characterization of the analyzed mortars. •• = abundant; • = frequent; - = sporadic; - - = extremely occasional.

Group	Samples	Lime	Porosity	Aggregates
A	T-ROM10, 13, 14, 18	carbonatic, micritic, homogeneous. Lime lumps (••); unburned limestones (-)	vughs, vesicles (••)	Quartz (••); Feldpars (•); Quartzites (•); Clasts of andesites/dacites (•); Calcarenite fr. (-); Shells (-); Crystalline limestone fr. (- -); Granitoids (- -); *Terracotta* fr. (- -); Carbonate sand (- -)
B	T-ROM8, 9, 19, 21	carbonatic, micritic, homogeneous. Lime lumps (•)	vughs, vesicles (••)	Quartz (••); Pyroclastic pozzolans (••); Feldspars (•); Quartzites (•); Clasts of andesites/dacites (-); Calcarenite fr. (- -); Shells (- -); Crystalline limestone fr. (- -); Carbonate sand (- -)

Group A gathers all the samples (T-ROM10, 13, 14, 18) collected from the western rooms of the building, exhibiting the same compositional and textural characteristics. They are 'fat' aerial lime mortars (approximately 1.5:1 binder to aggregate proportions), having a micritic lime binder with a homogeneous structure. There are numerous, multi-millimetric lumps of unmixed lime and some relicts of calcined fossiliferous calcarenites. The porosity is relevant (around 15%) and constituted by vughs/vesicles. The aggregate consists of locally sourced sand [26,27], moderately sorted and falling within the range of medium to coarse/very coarse sands (0.25–1.5 mm). From a petro-mineralogical point of view, the aggregate is primarily represented by quartz, with sporadic metamorphosed quartzites (Figure 4a). A subordinate fraction is made of clasts of plagioclase and K-feldspar (mainly orthoclase/microcline), often altered (Figure 4b) [28,29], fragments of local dacites/andesites (Figure 4c), sometimes displaying a feeble reaction rim with the surrounding lime, and fossiliferous calcarenites (Figure 4d). Carbonate clasts (fossiliferous and crystalline limestones) are present in lower amounts. Scattered bioclasts (bivalves and gastropods), granitoids, and small *terracotta* fragments have been also observed.

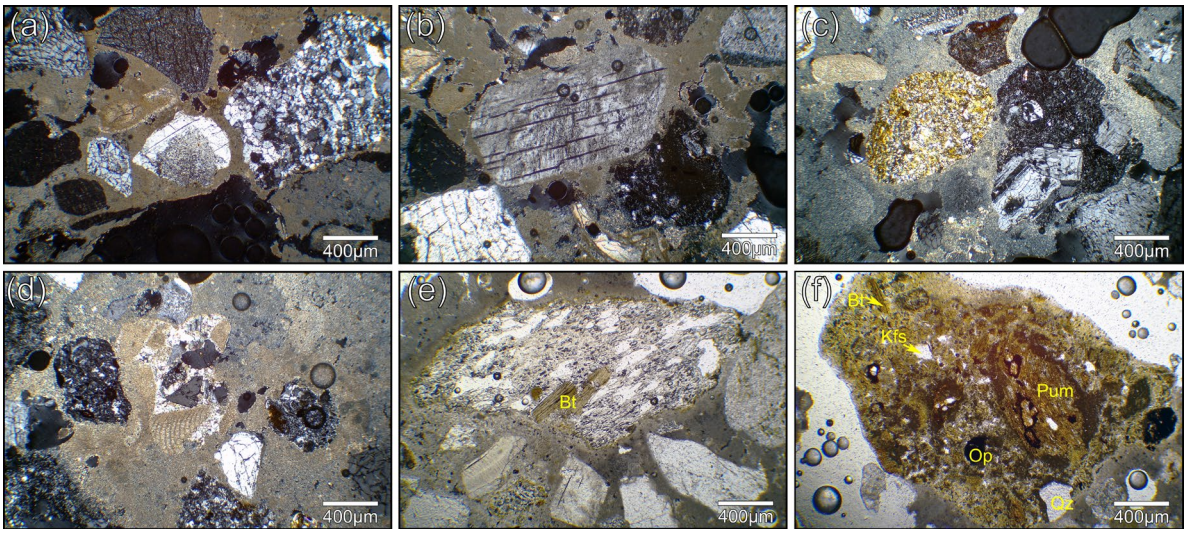

Figure 4. Detailed micrographs in Polarized Light Microscopy, in transmitted light (TL) crossed nicols (XN) and parallel nicols (PL); (**a**) clasts of quartz and quartzites (TL-XN); (**b**) a clast of altered K-feldspar in the center of the image (TL-XN); (**c**) on the right, a clast of volcanic rock, represented by local andesites/dacites (TL-XN); (**d**) in the center, a relict of fossiliferous calcarenite, surrounded by clasts of andesites/dacites (TL-XN); (**e**) a sub-millimetric clast of glassy pumice, with biotite (Bt) phenocrysts (TL-PN). (**f**) A sub-millimetric fragment of tuff with clasts of pumice and phenocrysts of biotite (Bt), K-feldspars (Kfs), opaque minerals (Op), and scattered quartz (Qz) (TL-PN).

Group B reunites all the samples (T-ROM8, 9, 19, 21) from the walls and foundations of the *cella*. These mortars differ from the above-mentioned group for the presence of volcanic pozzolan. More in detail, a relevant fraction of the pozzolanic aggregate is composed of pyroclastic rocks, having a pluri-millimetric/centimetric to sub-millimetric (from 0.5 mm upwards) grain size distribution, represented by scattered pumices (Figure 4e) and fragments of tuff (Figure 4f). They represent a finer fraction of the coarse clasts macroscopically observed in the structural mortars. Pumices display aphyric to porphyritic textures, with phenocrysts of biotite, anorthoclase, Ca-plagioclase, and K-feldspars (sanidine) and, rarely, clinopyroxenes. Tuffs present a cineritic matrix with fine-grained clasts of pumices, shards and scorias, phenocrysts of anorthoclase, Ca-plagioclase, K-feldspars (sanidine), biotite and occasionally clinopyroxenes, quartz, and opaque minerals. Both tuffs and pumices present feeble pozzolanic reactions with the lime binder, which appears carbonate-based, mi-critic, and rather homogeneous. Regarding the non-reactive fraction of the aggregate, in comparison with the mortars of group A, the presence of volcanic clasts (dacites/andesites) is feebly lower and terracotta fragments are absent. Lime lumps

are also sporadic. The estimated binder-to-aggregate proportions are around 1:1, due to the presence of the coarse clasts of volcanic pozzolan.

In the mortars of the Roman Temple, the clasts of volcanic pozzolan appear just feebly reacted. In fact, SEM-EDS analyses (Figure 5a,b) showed that in Group B mortars both tuff and pumice clasts are characterized by a substantially unaltered chemical profile, not only in the inner cores (Figure 5b1), but also in the interface areas, where, contrary to the expected results, calcium enrichment is negligible (Figure 5b2). In fact, chemical analyses of the matrix areas are characteristic of a highly calcic binder, with a limited occurrence of C-A-S-H (Figure 5b3). Due to the reduced reaction of volcanic pozzolans, the cementation index (C.I.) measured in the matrix areas of these samples is always less than 0.5, indicative of mortars with feeble to null hydraulic properties.

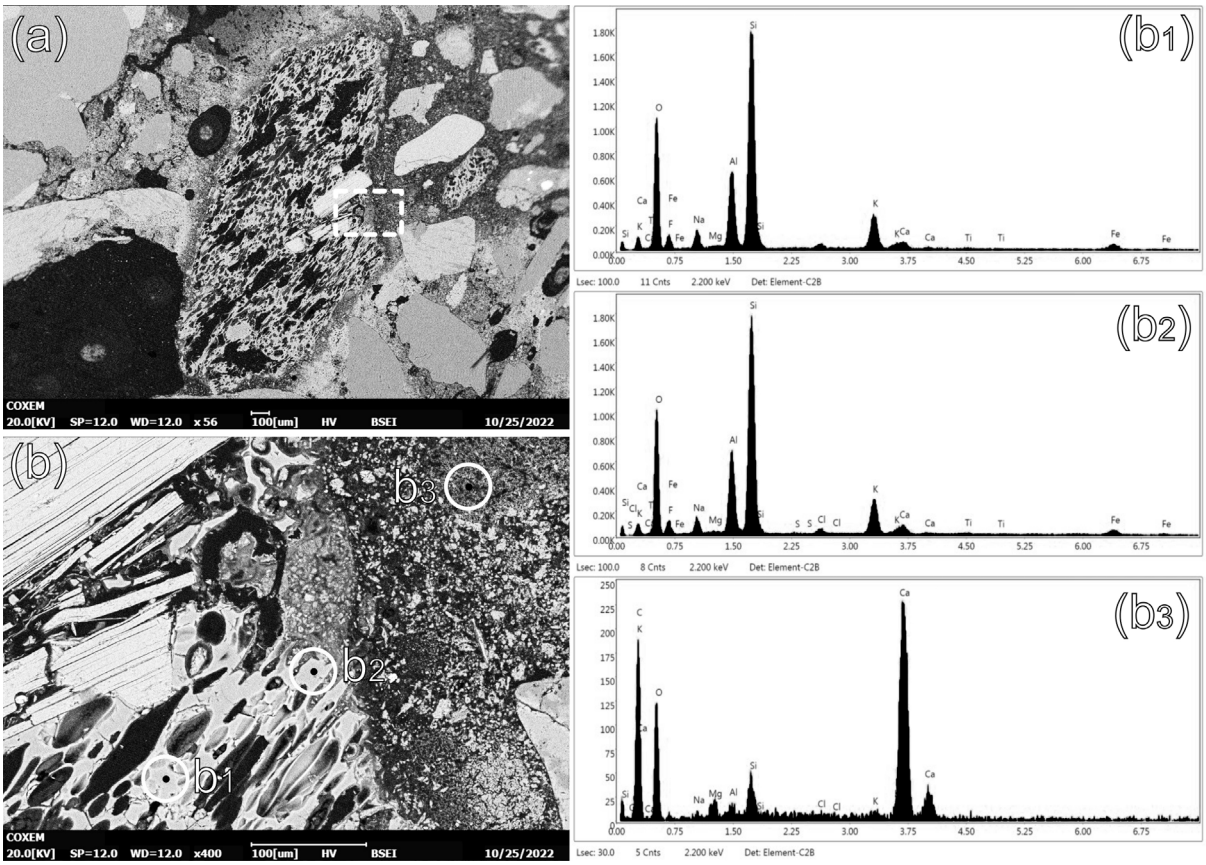

Figure 5. SEM-EDS analyses describing the reactivity of the volcanic pozzolan in mortars of group B: (**a**) a pumice clast in sample T-ROM8; (**b**) magnification of the dashed area in the Figure (**a**); (**b1**) EDS spectrum of the core of the pumice clasts; (**b2**) EDS spectrum of the interfacial area of the pumice clasts with the lime; (**b3**) EDS spectrum of a matrix area of the binder.

4.2. Minero-Chemical Characteristics and Provenance of the Pyroclastic Rocks

The minero-chemical characteristics and the provenance of the pyroclastic rocks were determined by combining QPA-XRPD and XRF analyses.

In accordance with the macroscopic observations of the cross sections, the cluster analysis (performed using the integrated function of Statgraphic Centurion PRO 18 software v. 18.1.12 (Statgraphics Technologies, Virginia, USA), based on the results of QPA-XRPD of the coarse clasts. The analysis was performed on the supposedly original mineralogical profile of volcanic samples, recalculated at 100% after the removal of alteration phases related to atmospheric pollution, namely, gypsum (sulphation) [30–32] and halite, likely derived from marine aerosol [33]. Calcite and, when detected, dolomite, were also removed as possibly related to lime intrusions (Table 3). The analysis reunited the coarse pozzolanic aggregates into two clusters having specific mineralogical patterns, the tuffs,

including samples T-ROM1 and T-ROM20, and the pumices, including samples T-ROM2, 3, 4, 5, 6, 7, 11 (Figure 6).

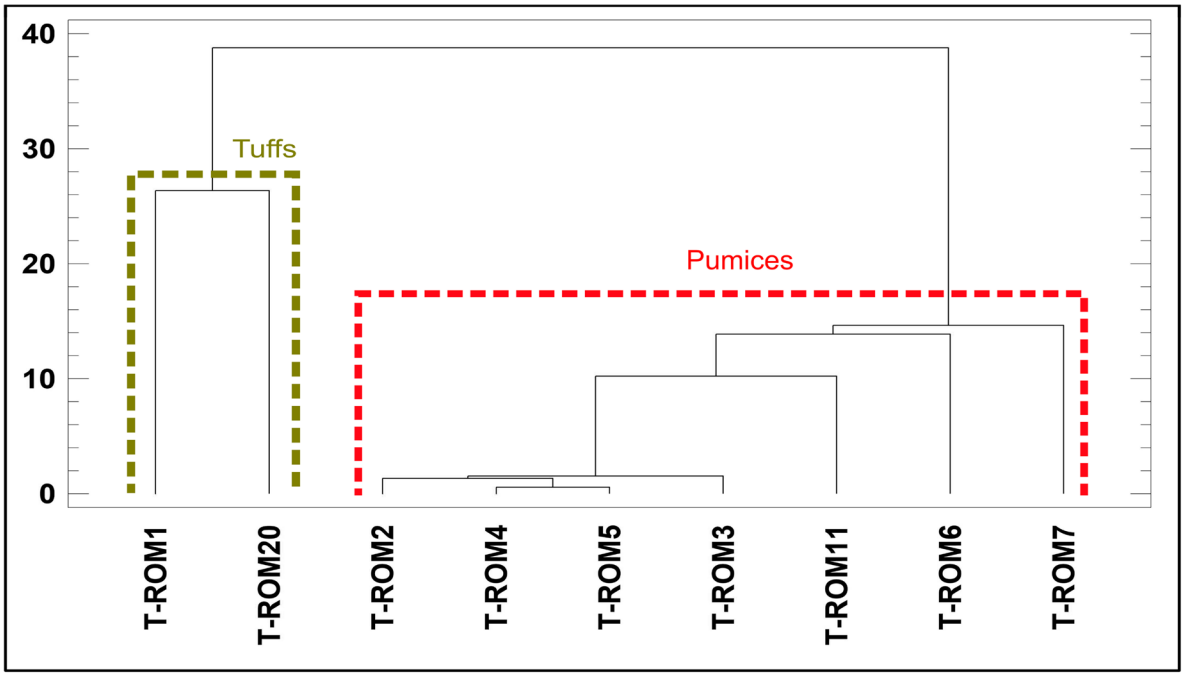

Figure 6. Results of the cluster analysis of the volcanic rock samples, based on XRPD-QPA data.

Table 3. QPA-XRPD of the analyzed volcanic clasts. b.d.l. = below detection limit.

														Alteration			
Sample	**Rock type**	**Biotite**	**Quartz**	**Na-plagioclase**	**Ca-plagioclase**	**K-feldspar**	**Clinopyroxene**	**Phillipsite**	**Chabazite**	**Analcime**	**Ilmenite**	**Smectite**	**Amorphous**	**Gypsum**	**Halite**	**Calcite**	**Dolomite**
T-ROM1	tuff	0.9	2.0	3.7	5.6	11.0	3.5	19.3	10.8	2.1	b.d.l.	9.2	30.2	0.9	0.6	0.3	b.d.l.
T-ROM2	pumice	0.3	0.6	0.5	4.2	5.5	1.7	1.7	b.d.l.	0.6	b.d.l.	b.d.l.	84.6	b.d.l.	0.3	0.1	b.d.l.
T-ROM3	pumice	0.6	0.6	3.5	2.7	0.7	1.7	b.d.l.	b.d.l.	0.6	b.d.l.	b.d.l.	85.4	b.d.l.	0.8	3.4	b.d.l.
T-ROM4	pumice	0.3	0.5	5.8	1.9	5.9	1.6	b.d.l.	b.d.l.	b.d.l.	b.d.l.	b.d.l.	82.5	b.d.l.	b.d.l.	1.7	b.d.l.
T-ROM5	pumice	0.1	0.4	6.4	2.9	7.3	1.9	b.d.l.	b.d.l.	b.d.l.	b.d.l.	b.d.l.	78.5	0.3	1.2	0.9	b.d.l.
T-ROM6	pumice	0.2	0.1	3.9	5.5	34.2	b.d.l.	b.d.l.	b.d.l.	b.d.l.	b.d.l.	b.d.l.	54.4	b.d.l.	0.6	1.1	b.d.l.
T-ROM7	pumice	0.7	0.2	32.9	3.0	14.0	3.7	2.1	b.d.l.	b.d.l.	b.d.l.	b.d.l.	43.3	b.d.l.	b.d.l.	0.2	b.d.l.
T-ROM11	pumice	0.5	0.8	1.3	4.4	11.3	1.1	b.d.l.	b.d.l.	0.2	b.d.l.	b.d.l.	78.3	b.d.l.	0.2	1.9	b.d.l.
T-ROM20	tuff	1.4	1.0	8.1	8.5	13.3	2.1	18.7	3.7	4.8	1.1	4.6	30.0	b.d.l.	0.4	2.0	0.2

Tuff samples are characterized by the lowest amorphous content (~30 wt%) of the dataset, the presence of smectite clay, and the abundant occurrence of zeolites, namely, phillipsite (~19%wt), prevailing over chabazite and analcime (Figure 7a). This zeolitized pattern is typical of the volcanic products of Roman Comagmatic Region with particular coincidences with the Phlegraean Fields. In fact, the strong prevalence of phillipsite over chabazite and analcime is fairly indicative of the later Phlegraean volcanic products, with particular reference to Neapolitan Yellow Tuff (NYT) [34–37].

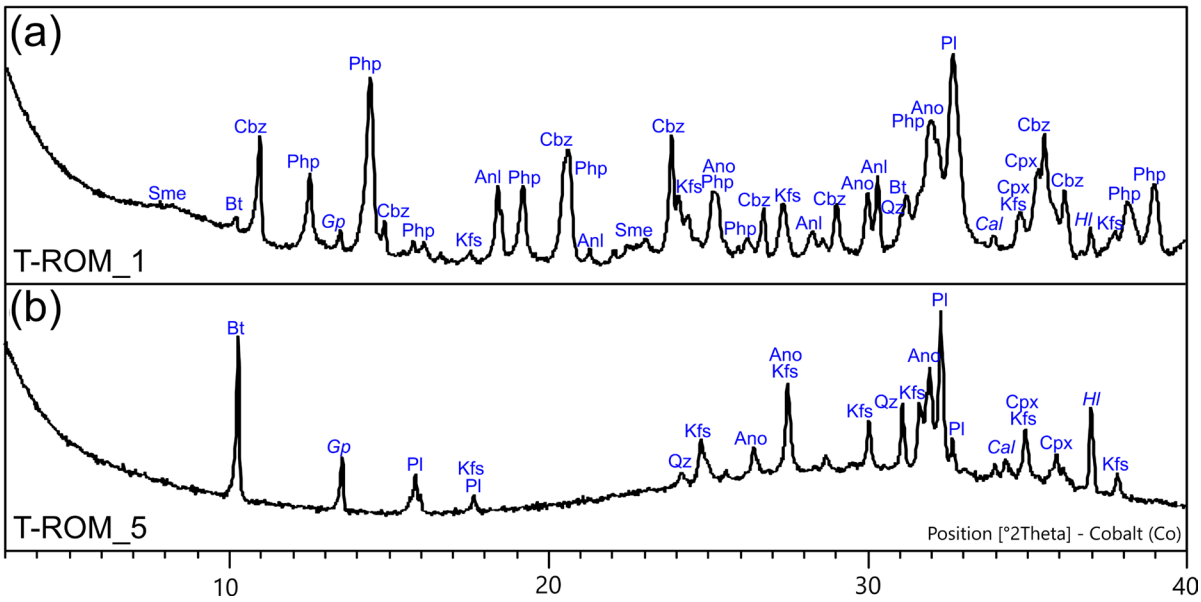

Figure 7. XRPD spectra of representative volcanic rock samples with an indication of peak phases (mineral abbreviations labeled according to [38]. The non-original rock-forming phases (binder intrusion, environmental pollution, marine salt) are indicated in italics: (**a**) XRPD spectrum of tuff sample T-ROM1; (**b**) XRPD spectrum of pumice sample T-ROM5.

Pumice samples are characterized by a high amorphous content, up to 80–90 wt% in some of the analyzed materials. The remaining phases primarily consist of a combination of K-feldspars, Na-plagioclases, and Ca-plagioclases, representing around 10–20 wt% of the samples (Figure 7b). These rates are inverted only in the pumice samples T-ROM6 and 7, where the amorphous fraction is lower (43–55 wt%), and equally proportioned to a crystalline component mainly constituted by feldspars (45–50 wt%). In these samples, the occurrence of zeolites, in particular phillipsite prevailing over analcime, was occasionally observed. In order to prove and confirm the provenance of the volcanic pozzolans suggested by QPA-XRPD data, their chemical characterization, determined by XRF (Table 4), was compared with the geochemical fingerprint of the volcanic products of the Plio-Quaternary eruptions of the Italian peninsula and islands.

Table 4. XRF profiles (bulk-rocks) of the analyzed volcanic clasts.

	T-ROM1	T-ROM2	T-ROM3	T-ROM4	T-ROM5	T-ROM6	T-ROM7	T-ROM11	T-ROM20
%Ox	tuff	pumice	pumice	pumice	pumice	pumice	pumice	pumice	tuff
SiO_2	59.31	60.29	60.89	60.82	60.53	61.71	60.5	60.07	62.07
TiO_2	0.48	0.47	0.49	0.53	0.46	0.44	0.47	0.45	0.44
Al_2O_3	18.29	18.55	18.45	18.30	18.38	18.26	18.89	18.41	17.75
Fe_2O_3	3.88	3.67	3.51	3.59	3.44	3.18	3.71	3.47	3.17
MnO	0.15	0.15	0.17	0.17	0.15	0.18	0.13	0.14	0.16
MgO	1.27	0.39	0.14	0.24	0.33	0.09	0.29	0.27	0.92
CaO	1.94	2.61	2.17	2.88	2.41	1.99	2.55	2.67	2.97
Na_2O	4.11	4.91	5.42	5.68	5.26	5.94	4.63	4.94	2.95
K_2O	9.30	8.00	7.63	7.41	8.01	7.15	8.52	8.23	9.25
P_2O_5	0.27	0.08	0.05	0.05	0.07	0.03	0.09	0.07	0.08
Tot	99.00	99.12	98.92	99.67	99.04	98.97	99.78	98.72	99.76
L.O.I.	14.97	4.96	3.55	3.76	3.48	2.34	3.38	3.27	11.71

	T-ROM1	**T-ROM2**	**T-ROM3**	**T-ROM4**	**T-ROM5**	**T-ROM6**	**T-ROM7**	**T-ROM11**	**T-ROM20**
ppm	tuff	pumice	pumice	pumice	pumice	pumice	pumice	pumice	tuff
S	169	137	38	126	76	63	56	95	145
Sc	3	<3	3	13	11	<3	3	<3	3
V	62	50	26	32	38	18	49	45	38
Cr	6	<6	4	<6	7	<6	5	<6	12
Co	3	9	<3	6	6	<3	<3	6	<3
Ni	5	<3	<3	<3	<3	<3	<3	<3	<3
Cu	33	9	17	217	143	24	24	31	10
Zn	103	102	100	106	126	109	89	411	81
Ga	12	18	13	14	14	17	10	12	13
Rb	362	390	436	440	411	478	381	392	366
Sr	223	203	127	81	110	45	278	152	196
Y	30	45	63	65	49	73	37	43	50
Zr	386	550	763	779	610	956	517	528	660
Nb	52	67	94	101	77	113	65	64	86
Ba	766	104	122	35	46	21	182	73	231
La	81	102	122	132	108	161	97	93	118
Ce	161	204	252	267	220	323	196	193	238
Nd	60	73	103	105	82	110	72	71	87
Pb	75	71	62	62	55	50	62	53	49
Th	43	49	72	74	56	89	50	52	67
U	8	16	22	20	18	26	14	15	16

From the TAS (Total Alkali vs. Silica) scatterplot [39], the clasts fall in the chemical intervals between trachyte and phonolite (Figure 8a). They overlap with the geochemical fingerprint of most of the volcanic units of the Neapolitan district, comprising the alkaline products of Phlegraean eruptions (mainly pyroclastic rocks), including the pre- and Campanian ignimbrite (pre-CI and CI) and the pre-, post-, and Neapolitan Yellow Tuff (pre-NYT, NYT, and post-NYT) activities, as well as the volcanoes of the islands of Ischia and Procida-Vivara (pyroclastic rocks), considered part of the Phlegraean volcanism (Figure 8b).

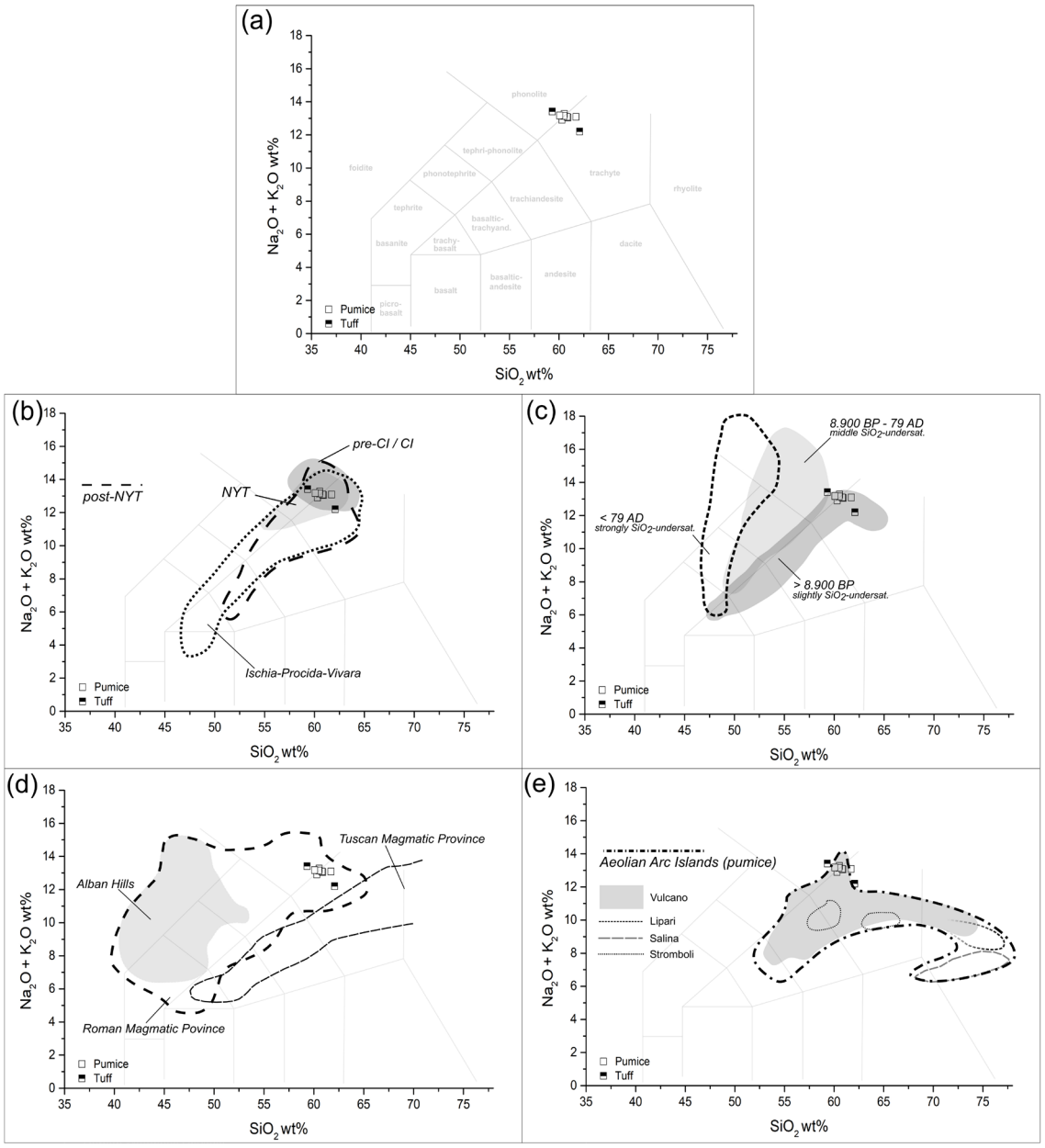

Figure 8. TAS (Total Alkali vs. Silica) scatterplots of coarse samples of pumices and tuffs from the Roman Temple of Nora in comparison with volcanic products of the Italian magmatic districts displaying petrochemical affinity: (**a**) Samples' distribution according to volcanic rocks' chemistry, after [39]; (**b**) samples' distribution according to rock chemistry of the products of the Campanian Ignimbrite (CI), Neapolitan Yellow Tuff (NYT), post-NYT and Ischia/Procida-Vivara volcanic activities (chemical fields edited from [40,41]; (**c**) samples' distribution in relation to the three main eruptive facies of the Somma-Vesuvius volcanic activities (compositional fields edited from [36,40,41]); (**d**) samples' distribution in relation to the fields occupied by the products of the Roman and Tuscan Magmatic provinces (compositional fields edited from [40,42]); (**e**) samples' distribution in relation to the fields occupied by the pyroclastic products of the Aeolian Arc Islands (compositional fields edited from [43].

On the basis of the TAS, the volcanic pozzolans of Nora overlap also with the fields of the alkaline and highly alkaline series of Somma-Vesuvius (Figure 8c). Some correspondences can be drawn also with certain trachy-phonolitic cinerites of the Roman Magmatic province, with the exception of the highly alkaline cinerites of the Colli Albani (*harenae fossiciae*) (Figure 8d), and with some pyroclastic rocks of the isles of the Aeolian Arc

[43] (Figure 8e), as the emissions of Vulcano island display a compatible trachytic chemism.

On the other hand, the chemical and petrographic features of the analyzed rocks are not compatible with the petrochemistry of most of the volcanic products of Sardinia [40,44] and, in particular, with the pyroclastic products of Mt. Arci and Sant'Antioco volcanoes, primarily constituted of rhyolitic/alkali-rhyolitic perlites and obsidians [40,44].

Considering the high variability of the TAS, following [5,6,11,45–48], indicative major (TiO_2) and trace elements (Zr, Nb, Y, and Th) were useful to track the origin of the pyroclastic rocks at a higher grade of accuracy, in particular for those pumice samples that do not display indicative mineral assemblages for the provenance determination.

On the basis of Nb/Zr, all clasts plot over the field of the volcanic products of Campania (Figure 9a).

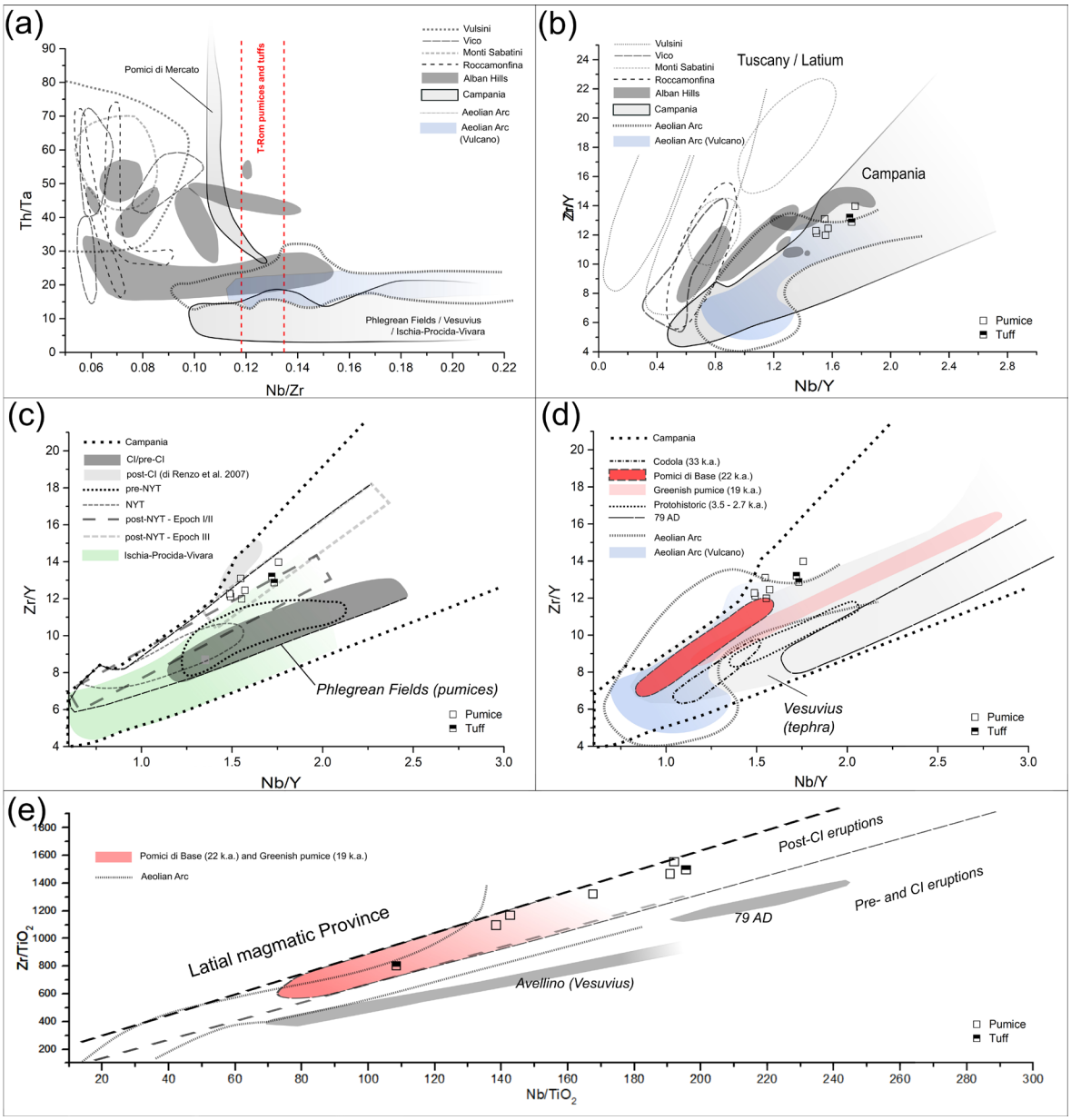

Figure 9. Trace elements' scatterplots of coarse samples of pumices and tuffs from the Roman Temple of Nora in comparison with volcanic products of the Italian magmatic districts displaying petrochemical affinity: (**a**) Nb/Zr vs. Th/Ta scatterplot of clasts' samples in relation to the fields occupied by the Roman, Tuscan, and Campanian magmatic provinces (compositional fields edited from [6,11,47,48] and Aeolian Arc Islands' volcanic products (chemical field based on raw data from

[43,49,50]); (**b**) Nb/Y vs. Zr/Y scatterplot of clasts' samples in relation to the fields occupied by the Roman, Tuscan, and Campanian magmatic provinces (compositional fields edited from [6,11,47,48]), the Aeolian Arc Island's products (compositional fields based on raw data from [43,49,50,51]; (**c**) Nb/Y vs. Zr/Y scatterplot of clasts' samples in relation to the fields occupied by volcanic products of the Phlegraean Fields main eruptions (according to [52,53]) of pre-CI (Campanian Ignimbrite), CI, post-CI, pre-NYT (Neapolitan Yellow Tuff), NYT, and post-NYT, distinguished into Epoch I/II and Epoch III (compositional fields edited from [6,11,47,48]), together with Phlegraean-correlated products (pumices and scorias) of Ischia/Procida-Vivara (compositional fields based on raw data from [54–58]); (**d**) Nb/Y vs. Zr/Y scatterplot of clasts' samples in relation to the fields occupied by volcanic products of Somma-Vesuvius main eruptions (79AD/pre-79AD, according to [59], compositional fields edited from [6]) and Aeolian Isles volcanic tephra (compositional fields based on raw data from [43,49,50,51]; (**e**) Nb/TiO_2 vs. Zr/TiO_2 scatterplot of clasts' samples in relation to the fields occupied by the Roman, Tuscan, and Campanian magmatic provinces (compositional fields edited from [6,11]) and the Aeolian Isle volcanic tephra (compositional fields based on raw data from [49–51].

The possibility of their provenance from most of the volcanic units of the Roman and Tuscan magmatic provinces can be excluded, as they systematically display Nb/Zr ratios <0.11. However, being Ta not acquired by XRF, in the scatterplot reported in Figure 9a, the volcanic clasts from Nora can be only described as an interval, having as maximum and minimum the lower and the higher Nb/Zr values, respectively. This area overlaps the fields of the Aeolian Arc and the Colli Albani volcanic products too. However, this latter district can be safely excluded as a possible procurement zone as demonstrated by TAS.

By the Zr/Y vs. Nb/Y scatterplots in Figure 9b, all the analyzed clasts systematically plot over the fields of the main volcanic units of Campania, with certain correspondences also with Aeolian Isles.

In detail, with regards to the Zr/Y vs. Nb/Y scatterplots in Figure 9c, all the clasts overlay the fields of the tephra of the Phlegraean eruptions with good matches with the younger products of the post-Neapolitan Yellow Tuff (<12 k.a.). Marginal overlaps can be detected with the pyroclastic products of the Phlegraean-correlated eruptions of Ischia and Procida-Vivara. On the other hand, all the analyzed clasts do not match the geochemical fingerprint of the pumices/ashes of Somma-Vesuvius, and some clasts display just a marginal overlap within the fields of the older Somma-Vesuvius eruptions (22 k.a. Pomici di Base). However, the provenance of most of the analyzed clasts from the volcanic deposits of the Neapolitan district is not straightforward, as some pumices in the Zr/Y vs. Nb/Y intervals overlap the fields of the Aeolian Arc volcanoes (Figure 9d), and possible geochemical affinities with Vulcano's pyroclastic products were also detected by TAS.

The Nb/TiO_2 vs. Zr/TiO_2 scatterplot in Figure 9e does not provide any further information to definitely distinguish the pyroclastic coarse clasts from Nora between the Somma-Vesuvius older eruptive series, post-CI Phlegraean products, and Aeolian Isle.

On the basis of these data, a possible provenance of at least some of the pozzolanic pumices from the Aeolian area cannot be undeniably ruled out, not even from a mere geographical point of view. In fact, the relative proximity of these Sicilian islands to the southern coast of Sardinia would have made a maritime trade of this raw material easy.

Therefore, in order to definitely ascertain at a higher grade of resolution the provenance of the volcanic pumices of Nora between the volcanic units of the Neapolitan district and the Aeolian isles (Vulcano), a discriminant analysis (performed using Statgraphic Centurion PRO 18 software) was performed adopting the descriptive geochemical profiles of geological pyroclastic compounds (i.e., pumices, ashes, and tephra) as the baseline on which the archaeological samples from Nora were compared.

A total of 405 geochemical profiles from the literature were used to develop a model to define the best geochemical compatibilities among the volcanic districts displaying possible geochemical affinity, i.e., the Phlegraean Fields (data from [46,60–67,52,68], distinguished into post-CI, Pre-NYT, NYT, and Post-NYT including Epoch I/II and III according

to [53]), Ischia and Procida/Vivara (data from [54–58]; Somma-Vesuvius (Pomici di Base eruption, data from [69,70]), Vulcano in the Aeolian Arc (data from [43,49]).

The discriminant factors are constituted by a pattern of indicative trace elements (Zr, Nb, Th, Rb, Sr, Y, Ba, La, Ce, and Nd) that were adequately measured by XRF or LA-ICP-MS in each one of the baseline's samples. These were classified a priori according to their known provenance. Ten variables were used, corresponding to the selected trace elements. Six discriminant functions were extracted having a P-value less than 0.05, statistically significant at the 95.0% confidence level. The classification scores and details are reported in Table 5.

Table 5. Coefficients of the classification function (trace elements) for each eruptive event.

Trace Element	Phlegraean Fields					Ischia	Procida-Vivara	Vesuvius	Aeolian Arc
	Post CI	Pre-NYT	NYT	Post-NYT (Epoch I/II)	Post-NYT (Epoch III)			Pomici di Base	Vulcano
Zr	0.06	0.03	0.03	0.06	0.04	0.03	0.02	0.05	−0.01
Nb	−0.64	−0.23	−0.42	−0.46	−0.33	−0.17	−0.21	−0.42	−0.28
Th	0.21	−0.15	−0.15	−0.04	−0.01	−0.43	−0.07	−0.09	0.31
Rb	0.23	0.17	0.24	0.21	0.19	0.16	0.13	0.21	0.17
Sr	0.04	0.03	0.04	0.04	0.04	0.02	0.03	0.04	0.05
Y	0.03	0.06	0.06	0.05	0.04	0.10	0.06	0.10	0.06
Ba	−0.01	−0.01	−0.01	−0.01	−0.01	0.00	−0.01	−0.01	−0.01
La	−0.12	−0.10	−0.12	−0.13	−0.11	−0.07	−0.06	−0.14	−0.02
Ce	−0.20	−0.18	−0.22	−0.26	−0.22	−0.20	−0.17	−0.23	−0.14
Nd	0.35	0.57	0.65	0.75	0.60	0.79	0.56	0.62	0.29
CONSTANT	−37.39	−27.17	−42.20	−40.89	−35.34	−34.11	−21.89	−37.65	−34.30

The results of the discriminant analysis demonstrated (at the two higher probability intervals) a high compatibility of the analyzed tuff and pumice samples from Nora with the volcanic products of the Neapolitan district, especially with the later (post-NYT) Phlegraean eruptions (Table 6). None of the clasts presents geochemical correspondences with the pyroclastic products of Ischia and Procida-Vivara, Somma-Vesuvius and Aeolian Arc. Therefore, by combining QPA-XRPD and XRF results, the Phlegraean fields can be proposed for the provenance of all the volcanic pozzolanas of the Roman Temple of Nora, with a strong association with the later Phlegraean formations (post-NYT).

Table 6. Provenance of the analyzed volcanic clasts from Nora according to the results of the discriminant analysis.

Sample	Rock Type	Provenance (1st Probability)	Provenance (2nd Probability)
T-ROM_1	tuff	Post-NYT (Epoch I/II)	NYT
T-ROM_2	pumice	Post-NYT (Epoch I/II)	NYT
T-ROM_3	pumice	Post-NYT (Epoch I/II)	Post-NYT (Epoch III)
T-ROM_4	pumice	Post-NYT (Epoch I/II)	Post-NYT (Epoch III)
T-ROM_5	pumice	Post-NYT (Epoch I/II)	Post-NYT (Epoch III)
T-ROM_6	pumice	Post-NYT (Epoch I/II)	Post-NYT (Epoch III)
T-ROM_7	pumice	Post-NYT (Epoch I/II)	Post-NYT (Epoch III)
T-ROM_11	pumice	Post-NYT (Epoch I/II)	NYT
T-ROM_20	tuff	Post-NYT (Epoch I/II)	Post-NYT (Epoch III)

5. Discussion and Conclusions

The data reported in the paper clearly demonstrate that the pyroclastic rocks used in the structural mortars of the so-called Roman Temple of Nora were entirely procured from the Bay of Naples. This evidence suggests several considerations for discussion.

Primarily, on the basis of the current state of the art regarding this specific topic, this is the first analytically validated case of utilization of Phlegraean volcanic pozzolans in Nora as well as in the entire Sardinia. Moreover, preliminary analytical studies possibly evidence that volcanic pozzolans with the same petrochemical features as those of the Roman Temple were employed in lime-based mortars of at least one other sacred building (Temple of Aesculapius), dating to the Middle Imperial age [71] and in the renders of several cisterns [72] of the ancient town. Therefore, the evidence from the Roman Temple is not isolated, and it is likely that a continuous and organized trade of volcanic pozzolans from the Bay of Naples to Nora was active in these centuries. The extension of the analysis to other Roman buildings of the ancient town (currently underway) will allow these hypotheses to be verified.

However, such commerce in materials appears outstanding, especially considering that analytical investigations performed in past years on the structural mortars of the theatre, an older building dated to the Augustan Age, demonstrated the presence of local volcanic pozzolans (rhyolitic obsidian and perlites) likely sourced from the Sardinian district of Monte Arci [73]. This change in the supply of pozzolanic material from intra-regional to extra-regional quarry areas in the Middle-Imperial Age is intriguing: the different provenance of the crafts operating in Nora during the Roman era together with the extension of the trading system of the Roman Empire, which reached its climax between the 2nd and 3rd c. AD, could have influenced this modification. In fact, at this time Nora was undergoing a great infrastructural and architectural urban renovation, highlighted by the adoption of innovative construction techniques, such as the brick facings and the *opus caementicium* structures, systematically employed in this period for the construction of the main monuments of the town [19,74].

A second point concerns the function of the structures in which the Campanian pozzolan was used. In fact, although the presence of *pulvis puteolana* in maritime infrastructures was evidenced in several contexts, its occurrence in the structural mortars of above-ground buildings appears common in the sites around the Bay of Naples [75–79], whereas it has not been clearly detected elsewhere so far, apart from some hints from North Africa to be investigated further [80,81]. However, the use in Nora of the *pulvis puteolana* in the mortars of the above-ground masonries of the Roman Temple—not related to the maritime environment—completely fulfills the aforementioned Vitruvian statement (2.6.1) regarding the use of the "prodigious powder" for structural reinforcement. This opens new questions about the construction reasons for which the demand and commercialization for this product was intended. In fact, considering the spatial distribution of pozzolana-rich samples (Group B), the use of the pyroclastic rocks in the Roman Temple had the specific function of improving the overall cohesive capacities of the mortars of the thick masonries of the *cella*, on which the static load was surely greater than in the thinner walls of the western rooms where, in fact, pozzolana-rich mortars are not attested (Group A samples).

However, as demonstrated by the analytical investigations, the use of feebly ground, slightly reacted, and inhomogeneously distributed volcanic pozzolanas in the compounds resulted in a technologically weak product, probably manufactured by under-experienced craftsmen. Therefore, the use of the high-quality *pulvis puteolana* was pointless and its binding potential was drastically reduced.

Author Contributions: Conceptualization: S.D., C.P., and J.B.; samplings: S.D. and C.P.; samples preparation: S.D.; samples analysis: S.D. in collaboration with D.M., R.D.L., and M.S.; interpretation of the archaeometrical results: S.D., C.P., and J.B.; supervision, J.B.; S.D. drafted Sections 1, 2.2, 3, and 4; A.Z. drafted Section 2.1; C.P., J.B., and S.D. drafted Section 5; A.Z. realized Figure 1; S.D.

realized Figures 2–9 and all the tables; S.D., C.P., J.B., A.Z., and M.S. collaborated to the revision of the manuscript. All authors have read and agreed to the published version of the manuscript.

Funding: The research project received partial financial support from the University of Padova, in the frame of the project "Archaeometric investigations on the Euganean Pozzolan" (principal investigator: M. Secco, BIRD 2020 of the Department of Cultural Heritage, project code: SECC_BIRD20_01).

Institutional Review Board Statement: Not applicable.

Informed Consent Statement: Not applicable.

Data Availability Statement: The data presented in this study are available on request from the corresponding author.

Acknowledgments: The sampling was carried out during the excavation campaigns of the Department of Cultural Heritage of the University of Padova at the Roman Temple of Nora (2008-2014) under a convention and joint agreement with the Archaeological Superintendence of Cagliari and Oristano.

Conflicts of Interest: The authors declare no conflict of interest.

References

1. Lancaster, L.C. Pozzolans in Mortar in the Roman Empire: An Overview and Thoughts on Future Work. In *Mortiers et Hydraulique en Méditerranée Antique*; Ortega, F., Bouffier, S.; Eds.; Archéologies Méditerranéennes 6; Presses Universitaires de Provence: Aix-en-Provence, France, 2019; pp. 31–39.
2. Cook, D.J. Natural pozzolanas. In *Cement Replacement Materials*; Swamy, R.N., Ed.; Surrey University Press: London, UK, 1986; pp. 1–39.
3. Massazza, F. Pozzolana and Pozzolanic Cements. In *Lea's Chemistry of Cement and Concrete*; Hewlett, P.C., Ed.; Arnold: London, UK; Wiley: New York, NY, USA, 1998; pp. 471–635.
4. Dilaria, S.; Secco, M.; Bonetto, J.; Ricci, G.; Artioli, G. Making ancient mortars Hydraulic. How composition influences type and structure of reaction products. In Proceedings of the 6th Historic Mortar Conference, Ljubljana, Slovenia, 21–23 September 2022; Bokan Bosiljkov, V., Padovnik, A., Turk, T., Štukovnik, P., Eds.; pp. 55–69.
5. Brandon, C.J.; Hohlfelder, R.L.; Jackson, M.D.; Oleson, J.P. (Eds.) *Building for Eternity. The History and Technology of Roman Concrete Engineering in the Sea*; Oxbow Books: Philadelphia, PA, USA, 2014.
6. Marra, F.; Anzidei, M.; Benini, A.; D'Ambrosio, E.; Gaeta, M.; Ventura, G.; Cavallo, A. Petro-chemical features and source areas of volcanic aggregates used in ancient Roman maritime concretes. *J. Volcanol. Geotherm. Res.* **2016**, *328*, 59–69.
7. Secco, M.; Asscher, Y.; Ricci, G.; Tamburini, S.; Preto, N.; Sharvit, J.; Artioli, G. Cementation processes of Roman pozzolanic binders from Caesarea Maritima (Israel). *Constr. Build. Mater.* **2022**, *355*, 129128.
8. Gros, P.; Corso, A.; Romano, E. (Eds.) *Vitruvio, De Architectura*; G. Einaudi: Torino, Italy, 1997.
9. Giuliani, C.F. *L'edilizia nell'antichità*; Carocci: Roma, Italy, 2006.
10. Adam, J.-P. *Roman building. Materials and Techniques*; Routledge: London, UK; New York, NY, USA, 1997.
11. D'Ambrosio, E.; Marra, F.; Cavallo, A.; Gaeta, M.; Ventura, G. Provenance materials for Vitruvius *harenae fossiciae* and *pulvis puteolanis*: Geochemical signature and historical-archaeological implications. *J. Archaeol. Sci. Rep.* **2015**, *2*, 186–203.
12. Lancaster, L.C. Mortars and plasters—How mortars were made. The literary sources. *Archaeol. Anthropol. Sci.* **2021**, *13*, 192.
13. Bonetto, J. Nora fenicia. Nuovi dati e nuove letture. In *Tra le Coste del Levante e le Terre del Tramonto. Studi in Ricordo di Paolo Bernardini*; Bondì, S.F., Botto, M., Garbati, G., Oggiano, I., Eds.; Collezione di Studi Fenici 51; Quasar: Roma, Italy, 2021; pp. 195–208.
14. Bonetto, J. Nora nel V secolo: dall'emporio fenicio a colonia cartaginese. In *La Sardegna, il Mediterraneo occidentale e Cartagine nel V secolo a.C.*; Roppa, A., Botto, M., Van Dommelen, P., Eds.; Quasar: Roma, Italy, 2021; pp. 91–106.
15. Ghiotto, A.R.; Zara, A. Nora tra III e I secolo a.C.: La graduale transizione da città punica a città romana. In *Nora Antiqua, II. Nora dalla Costituzione della PROVINCIA all'età Augustea*; Atti del Convegno di Studi (Pula, 5–6 ottobre 2018); Scavi di Nora IX; Bonetto, J., Carboni, R.; Giuman, M., Zara, A., Eds.; Quasar: Roma, Italy, 2020; pp. 3–18.
16. Asolati, M.; Bonetto, J.; Zara, A. Un deposito rituale di antoniniani dal settore orientale dell'abitato di Nora (Sardegna). *Annali. Ist. Ital. Numis.* **2018**, *64*, 99–146.
17. Zara, A. Il Tempio romano di Nora. Riflessioni sulla dedica in base a un frammento epigrafico inedito. In *L'Africa Romana. Momenti di Continuità e Rottura: Bilancio di Trent'anni di Convegni*; Atti del XX convegno internazionale di studi (Alghero-Porto Conte Ricerche, 26–29 settembre 2013); Ruggeri, P., ed.; Carocci: Roma, Italy, 2015; pp. 1889–1902.
18. Bonetto, J.; Mantovani, V.; Zara, A. (Eds.) *Nora. Il Tempio Romano (2008–2014). II.1. I Materiali Preromani. II.2. I Materiali Romani e Gli Altri Reperti*; Scavi di Nora X; Quasar: Roma, Italy, 2021.
19. Ghiotto, A.R. *L'architettura Romana Nelle Città della Sardegna*; Quasar: Roma, Italy, 2004.
20. Schneider, C.A.; Rasband, W.S.; Eliceiri, K.W. NIH Image to ImageJ: 25 years of image analysis. *Nat. Methods* **2012**, *9*, 671–675.

21. Boynton, R.S. *Chemistry and Technology of Lime and Limestone*; Interscience Publ. J. Wiley: New York, NY, USA, 1966.
22. Charola, A.E.; Henriques, F.M.A. Hydraulicity in lime mortars revisited. In *Historic Mortars: Characteristics and Tests: Proceedings of a RILEM Workshop, Paisley, (12–14/05/1999)*; Bartos, P., Groot, C., Hughes, J.J., Eds.; RILEM: Cachan Cedex, France, 2000; pp. 95–104.
23. Rietveld, H.M. Line Profiles of Neutron Powder-diffraction Peaks for Structure Refinement. *Acta Crystallogr.* **1967**, *22*, 151–152.
24. Taut, T.; Kleeberg, R.; Bergmann, J. The new Seifert Rietveld program BGMN and its application to quantitative phase analysis. *Mater. Struct.* **1998**, *5*, 55–64.
25. Dollase, W. Correction of Intensities for Preferred Orientation in Powder Diffractometry: Application of the March Model. *J. Appl. Crystallogr.* **1986**, *19*, 267–272.
26. Melis, S.; Columbu, S. Les matériaux de construction à l'époque romaine et leur rapport avec les anciennes carrières: l'exemple du théâtre de Nora (Sardaigne SO—Italie). In *La pierre dans la ville antique et médiévale, Actes du colloque d'Argentomagus Tours (Argenton-sur-Creuse, Saint-Marcel, 30–31/03/1998)*; Lorenz, J., Tardy, D., Coulon, G., Eds.; Supplément à la Revue ar-chéologique du centre de la France, 18; Musee d'Argentomagus: Saint-Marcel, France, 2000; pp. 103–117.
27. Columbu, S. Petrographic and geochemical investigations on the volcanic rocks used in the Punic-Roman archaeological site of Nora (Sardinia, Italy). *Environ. Earth Sci.* **2018**, *77*, 577.
28. Columbu, S.; Garau, A.M. Mineralogical, petrographic and chemical analysis of geomaterials used in the mortars of Roman Nora theatre (south Sardinia, Italy). *Ital. J. Geosci.* **2017**, *136*, 238–262.
29. Sitzia, F.; Beltrame, M.; Lisci, C.; Mirão, J. Micro Destructive Analysis for the Characterization of Ancient Mortars: A Case Study from the Little Roman Bath of Nora (Sardinia, Italy). *Heritage* **2021**, *4*, 2544–2562.
30. Sabbioni, C.; Zappia, G.; Riontino, C.; Blanco-Varela, M.T.; Aguilera, J.; Puertas, F.; Van Balen, F.; Toumbakari, E. Atmospheric deterioration of ancient and modern hydraulic mortars. *Atmos. Environ.* **2001**, *35*, 539–548.
31. Secco, M.; Previato, C.; Addis, A.; Zago, G.; Kamsteeg, A.; Dilaria, S.; Canovaro, C.; Artioli, G.; Bonetto, J. Mineralogical clustering of the structural mortars from the Sarno Baths, Pompeii: A tool to interpret construction techniques and relative chronologies. *J. Cult. Herit.* **2019**, *40*, 265–273.
32. Dilaria, S.; Previato, C.; Secco, M.; Busana, M.S.; Bonetto, J.; Cappellato, J.; Ricci, G.; Artioli, G.; Tan, P. Phasing the history of ancient buildings through PCA on mortars' mineralogical profiles: The example of the Sarno Baths (Pompeii). *Archaeometry.* 2022.
33. Secco, M.; Dilaria, S.; Bonetto, J.; Addis, A.; Tamburini, S.; Preto, N.; Ricci, G.; Artioli, G. Technological transfers in the Mediterranean on the verge of the Romanization: Insights from the waterproofing renders of Nora (Sardinia, Italy). *J. Cult. Herit.* **2020**, *44*, 63–82.
34. De' Gennaro, M.; Cappelletti, P.; Langella, A.; Perrotta, A.; Scarpati, C. Genesis of zeolites in the Neapolitan Yellow Tuff: Geological, volcanological and mineralogical evidence. *Contrib. Mineral. Petrol.* **2000**, *139*, 17–35.
35. Colella, A.; Calcaterra, D.; Cappelletti, P.; Langella, A.; Papa, L.; de' Gennaro, M. I tufi zeolitizzati nell'architettura della Campania. In *La Diagnostica per il Restauro del Patrimonio Culturale*; Cuzzolin: Napoli, Italy, 2009; pp. 327–341.
36. Morra, V.; Calcaterra, D.; Cappelletti, P.; Colella, A.; Fedele, L.; De' Gennaro, R.; Langella, A.; Mercurio, M.; De' Gennaro, M. Urban geology: Relationships between geological setting and architectural heritage of the Neapolitan area. *J. Virtual Explor.* **2010**, *36*, 1–60.
37. Langella, A.; Calcaterra, D.; Cappelletti, P.; Colella, A.; D'Albora, M.P.; Morra, V.; De Gennaro, V. Lava stones from Neapolitan volcanic districts in the architecture of Campanian region, Italy. *Environ. Earth Sci.* **2009**, *59*, 145–160.
38. Whitney, D.L.; Evans, B.W. Abbreviations for names of rock-forming minerals. *Am. Mineral.* **2010**, *95*, 185–187.
39. Le Bas, M.J.R.; Le Maitre, W.; Streckeisen, A.; Zanettin, B. IUGS Subcommission on the Systematics of Igneous Rocks, A Chemical Classification of Volcanic Rocks Based on the Total Alkali-Silica Diagram. *J. Petrol.* **1986**, *27*, 745–750.
40. Peccerillo, A. *Plio-Quaternary Volcanism in Italy: Petrology, Geochemistry, Geodynamics*; Springer: Berlin, Germany, 2005.
41. Peccerillo, A. Campania volcanoes. In *Vesuvius, Campi Flegrei, and Campanian Volcanism*; De Vivo, B., Belkin, H.E., Rolandi, G., Eds.; Elsevier: Amsterdam, Holland, 2020; pp. 79–120.
42. Avanzinelli, R.; Lustrino, M.; Mattei, M.; Melluso, L.; Conticelli, S. Potassic and ultrapotassic magmatism in the cir-cum-Tyrrhenian region: Significance of carbonated pelitic vs. pelitic sediment recycling at destructive plate margins. *Lithos* **2009**, *113*, 213–227.
43. Albert, P.G.; Tomlinson, E.L.; Smith, V.C.; Di Traglia, F.; Pistolesi, M.; Morris, A.; Donato, P.; De Rosa, R.; Sulpizio, R.; Keller, J.; et al. Glass geochemistry of pyroclastic deposits from the Aeolian Islands in the last 50 ka: A proximal database for tephrochronology. *J. Volcanol. Geotherm. Res.* **2017**, *336*, 81–107.
44. Lustrino, M.; Melluso, L.; Morra, V. The geochemical peculiarity of "Plio-Quaternary" volcanic rocks of Sardinia in the cir-cum-Mediterranean area. In *Cenozoic Volcanism in the Mediterranean Area*; Special Paper; Beccaluva, L., Bianchini, G., Wilson, M., Eds.; Geo-logical Society of America: Boulder, CO, USA, **2007**, *418*, 277–301.
45. Marra, F.; Deocampo, D.; Jackson, M.D.; Ventura, G. The Alban Hills and Monti Sabatini volcanic products used in ancient Roman masonry (Italy): An integrated stratigraphic, archaeological, environmental and geochemical approach. *Earth Sci. Rev.* ***2011***, *108*, 115–136.
46. Marra, F.; D'Ambrosio, E.; Sottili, G.; Ventura, G. Geochemical fingerprints of volcanic materials: Identification of a pumice trade route from Pompeii to Rome. *Bull. Geol. Soc. Am.* **2013**, *125*, 556–577.

47. Lancaster, L.C.; Sottili, G.; Marra, F.; Ventura, G. Provenancing of lightweight volcanic stones used in ancient Roman concrete vaulting: Evidence from Rome. *Archaeometry* **2011**, *53*, 707–727.
48. Marra, F.; D'Ambrosio, E. Trace element classification diagrams of pyroclastic rocks from the volcanic districts of central Italy: The case study of the ancient Roman ships of Pisa. *Archaeometry* **2013**, *55*, 993–1019.
49. Gioncada, A.; Mazzuoli, R.; Bisson, M.; Pareschi, M.T. Petrology of volcanic products younger than 42 ka on the Lipari-Vulcano complex (Aeolian Islands, Italy): An example of volcanism controlled by tectonics. *J. Volcanol. Geotherm. Res.* **2003**, *122*, 191–220.
50. De Astis, G.; La Volpe, L.; Peccerillo, A.; Civetta, L. Volcanological and petrological evolution of Vulcano island (Aeolian Arc, southern Tyrrhenian Sea). *J. Geophys. Res.* **1997**, *102*, B4, 8021-8050.
51. Davì, M.; De Rosa, R.; Donato, P.; Sulpizio, R. The Lami pyroclastic succession (Lipari, Aeolian Islands): A clue for unravelling the eruptive dynamics of the Monte Pilato rhyolitic pumice cone. *J. Volcanol. Geotherm. Res.* **2011**, *201*, 285–300.
52. Pappalardo, L., Civetta, L.; D'Antonio, M.; Deino, A.; Di Vito, M.A.; Orsi, G.; Carandente, A.; De Vita, S.; Isaia, R.; Piochi, M. Chemical and Sr isotopical evolution of the Phlegraean magmatic system before the Campanian Ignimbrite and the Neapolitan Yellow Tuff eruptions. *J. Volcanol. Geotherm. Res.* **1999**, *91*, 141–166.
53. Fedele, L.; Insinga, D.D.; Calvert, A.T.; Morra, V.; Perrotta, A.; Scarpati, C. 40Ar/39Ar dating of tuff vents in the Campi Flegrei caldera (southern Italy): Toward a new chronostratigraphic reconstruction of the Holocene volcanic activity. *Bull. Vol-Canology* **2011**, *73*, 1323–1336.
54. Poli, S.; Chiesa, S.; Gillot, P.-Y.; Gregnanin, A.; Guichard, F. Chemistry versus time in the volcanic complex of Ischia (Gulf of Naples, Italy): Evidence of successive magmatic cycles. *Contrib. Mineral. Petrol.* **1987**, *95*, 322–335.
55. De Astis, G.; Pappalardo, L.; Piochi, M. Procida volcanic history: New insights into the evolution of the Phlegrean Volcanic Discrict (Campania Region, Italy). *Bull. Volcanol.* **2004**, *66*, 622–641.
56. Brown, R.J.; Orsi, G.; De Vita, S. New insights into Late Pleistocene explosive volcanic activity and caldera formation on Ischia (southern Italy). *Bull. Volcanol.* **2008**, *70*, 583–603.
57. Tomlinson, E.L.; Albert, P.G.; Wulf, S.; Brown, R.J.; Smith, V.C.; Keller, J.; Orsi, G.; Bourne, A.J.; Menzies, M.A. Age and geochemistry of tephra layers from Ischia, Italy: Constraints from proximal-distal correlations with Lago Grande di Monticchio. *J. Volcanol. Geotherm. Res.* **2014**, *287*, 22–39.
58. Melluso, L.; Morra, V.; Guarino, V.; De' Gennaro, R.; Franciosi, L.; Grifa, C. The crystallization of shoshonitic to peralkaline trachyphonolitic magmas in a H_2O–Cl–F-rich environment at Ischia (Italy), with implications for the feeder system of the Campania Plain volcanoes. *Lithos* **2014**, *210–211*, 242–259.
59. Santacroce, R.; Cioni, R.; Marianelli, P.; Sbrana, P.; Sbrana, A.; Sulpizio, R.; Zanchetta, G.; Donahue, D.J.; Joron, J.L. Age and whole rock-glass compositions of proximal pyroclastics from the major explosive eruptions of Somma-Vesuvius: A review as a tool for distal tephrostratigraphy. *J. Volcanol. Geotherm. Res.* **2008**, *177*, 1–18.
60. Orsi, G.; Civetta, L.; D'Antonio, M.; Di Girolamo, P.; Piochi, M. The Neapolitan Yellow Tuff, a large-magnitude trachytic phreatoplinian eruption: Eruptive dynamics, magma withdrawal and caldera collapse. *J. Volcanol. Geotherm. Res.* **1992**, *67*, 291–312.
61. Pabst, S.; Wörner, G.; Civetta, L.; Tesoro, R. Magma chamber evolution prior to the Campanian Ignimbrite and Neapolitan Yellow Tuff eruptions (Campi Flegrei, Italy). *Bull. Volcanol.* **2008**, *70*, 961–976.
62. Di Vito, M.A.; Sulpizio, R.; Zanchetta, G.; D'Orazio, M. The late Pleistocene pyroclastic deposits of the Campanian Plain: New insights into the explosive activity of Neapolitan volcanoes. *J. Volcanol. Geotherm. Res.* **2008**, *177*, 19–48.
63. Di Vito, M.A.; Arienzo, I.; Braia, G.; Civetta, L.; D'Antonio, M.; Di Renzo, V.; Orsi, G. The Averno 2 fissure eruption: A recent small-size explosive event at the Campi Flegrei Caldera (Italy). *Bull. Volcanol.* **2011**, *73*, 295–320.
64. Di Renzo, V.; Di Vito, M.A.; Arienzo, I.; Caradente, A.; Civetta, L.; D'Antonio, M.; Giordano, F.; Orsi, G.; Tonarini, S. Magmatic history of Somma-Vesuvius on the basis of new geochemical and isotopic data from a deep borehole (Camaldoli della Torre). *J. Petrol.* **2007**, *48*, 758–784.
65. Tonarini, S.; D'Antonio, M.; Di Vito, M.A.; Orsi, G.; Carandente, A. Geochemical and B-Sr-Nd isotopic evidence for mingling and mixing processes in the magmatic system that fed the Astroni volcano (4.1–3.8 ka) within the Campi Flegrei caldera (southern Italy). *Lithos* **2009**, *107*, 135–151.
66. Smith, V.C.; Isaia, R.; Pearce, N.J.G. Tephrostratigraphy and glass compositions of post-15 kyr Campi Flegrei eruptions: Implications for eruption history and chronostratigraphic markers. *Quat. Sci. Rev.* **2011**, *30*, 3638–3660.
67. Tomlinson, E.L.; Arienzo, I.; Civetta, L.; Wulf, S.; Smith, V.C.; Hardiman, M.; Lane, C.S.; Carandente, A.; Orsi, G.; Rosi, M.; et al. Geochemistry of the Phlegraean Fields (Italy) proximal sources for major Mediterranean tephras: Implications for the dispersal of Plinian and co-ignimbritic components of explosive eruptions. *Geochim. Cosmochim. Acta* **2012**, *93*, 102–128.
68. Arienzo, I.; Mazzeo, F.C.; Moretti, R.; Cavallo, A.; D'Antonio, M. Open-system magma evolution and fluid transfer at Campi Flegrei caldera (Southern Italy) during the past 5 ka as revealed by geochemical and isotopic data: The example of the Nisida eruption. *Chem. Geol.* **2016**, *427*, 109–124.
69. Piochi, M.; Ayuso, R.A.; De Vivo, B.; Somma, R. Crustal contamination and crystal entrapment during polybaric magma evolution at Mt. Somma–Vesuvius volcano, Italy: Geochemical and Sr isotope evidence. *Lithos* **2006**, *86*, 303–329.
70. Ayuso, R.; De Vivo, B.; Rolandi, G.; Seal, R.; Paone, A. Geochemical and isotopic (Nd-Pb-Sr-O) variations bearing on the genesis of volcanic rocks from Vesuvius, Italy. *J. Volcanol. Geotherm. Res.* **1998**, *82*, 53–78.
71. Dilaria, S.; Marinello, A.; Zara, A. Analisi archeometriche delle malte aeree e pozzolaniche del tempio di Esculapio. *Risult. Prelim. Quad. Norensi* **2022**, *9*, 225–238.

72. Bonetto, J.; Dilaria, S. Circolazione di maestranze e saperi costruttivi nel Mediterraneo antico. Il caso dei rivestimenti in malta delle cisterne punico-romane di Nora (Cagliari, Sardegna). ATTA, Atlante tematico di Topografia Antica **2021**, *31*, 495–520.
73. Columbu, S.; Garau, A.M.; Lugliè, C. Geochemical characterisation of pozzolanic obsidian glasses used in the ancient mortars of Nora Roman theatre (Sardinia, Italy): Provenance of raw materials and historical–archaeological implications. *Archaeol. Anthropol. Sci.* **2019**, *11*, 2121–2150.
74. Previato, C. Building Public Baths outside Rome: The case study of Nora (Sardinia). In *Architectures of the Roman World. Models, Agency, Reception*; Mugnai, N., Ed.; *in press*.
75. Rispoli, C.; Graziano, S.F.; Di Benedetto, C.; De Bonis, A.; Guarino, V.; Esposito, R.; Morra, V.; Cappelletti, P. New insights of historical mortars beyond Pompei: The example of villa del Pezzolo, Sorrento peninsula. *Minerals* **2019**, *9*, 575.
76. Rispoli, C.; De Bonis, A.; Guarino, V.; Sossio, F.G.; Di Benedetto, C.; Esposito, R.; Morra, V.; Cappelletti, P. The ancient pozzolanic mortars of the Thermal complex of Baia (Campi Flegrei, Italy). *J. Cult. Herit.* **2019**, *40*, 143–154.
77. Montesano, G.; Verde, M.; Columbu, S.; Graziano, S.F.; Guerriero, L.; Iadanza, M.L.; Manna, A.; Rispoli, C., Cappelletti, P. Ancient Roman mortars from Anfiteatro Flavio (Pozzuoli, Southern Italy): A mineralogical, petrographic and chemical study. *Coatings* **2022**, *12*, 1712.
78. De Luca, R.; Miriello, D.; Pecci, A.; Domínguez-Bella, S.; Bernal-Casasola, D.; Cottica, D.; Bloise, A.; Crisci, G.M. Archaeometric study of mortars from the Garum Shop at Pompeii, Campania, Italy. *Geoarchaeology* **2015**, *30*, 330–351.
79. Miriello, D.; Barca, D.; Bloise, A.; Ciarallo, A.; Crisci, G.M.; De Rose, T.; Gattuso, C.; Gazineo, F.; La Russa, M.F. Characterisation of archaeological mortars from Pompeii (Campania, Italy) and identification of construction phases by compositional data analysis. *J. Archaeol. Sci.* **2010**, *37*, 2207–2223.
80. Pompilio, M. Inerti di natura vulcanica nei calcestruzzi del ninfeo ovest presso il Calcidico di Leptis Magna. In *Fontane e Ninfei minori di Leptis Magna*; Tomasello, F., Ed.; L'"Erma" di Bretschneider: Roma, Italy, 2005; pp. 290–291.
81. Djerad, M.S.; Boufenara, K.; des Courtils, J.; Cantin, N.; Lefrais, Y. Multianalytical characterisation and provenance investigation of natural pozzolana in Roman lime mortars from the archaeological site of Hippo Regius (Algeria). *Mediterr. Ar-Chaeology Archaeom.* **2022**, *22*, 231–248.

Disclaimer/Publisher's Note: The statements, opinions and data contained in all publications are solely those of the individual author(s) and contributor(s) and not of MDPI and/or the editor(s). MDPI and/or the editor(s) disclaim responsibility for any injury to people or property resulting from any ideas, methods, instructions or products referred to in the content.